# Same principle, but different computations in representing time and space

Sepehr Sima[1], Mehdi Sanayei[1]

**Author affiliations:**

[1]School of Cognitive Sciences, Institute for Research in Fundamental Sciences (IPM), Tehran, Iran

Correspondence to: Mehdi Sanayei

Full address: School of Cognitive Sciences, Institute for Research in Fundamental Sciences (IPM), Artesh Highway, Tehran, Iran, 19568-36484

mehdi.sanayei@gmail.com

**Abstract**

Time and space are two intertwined contexts that frame our cognition of the world and have shared mechanisms. A well-known theory on this case is ‘A Theory of Magnitude (ATOM)’ which states that the perception of these two domains shares common mechanisms. However, evidence regarding shared computations of time and space is intermixed. To investigate this issue, we asked human subjects to reproduce time and distance intervals with saccadic eye movements in similarly designed tasks. We applied an observer model to both modalities and found underlying differences the processing of time and space. While time and space computations are both probabilistic, adding prior to space perception minimally improved model performance, as opposed to time perception which was consistently better explained by Bayesian computations. We also showed that while both measurement and motor variability were smaller in distance than time reproduction, only the motor variability was correlated between them, as both tasks used saccadic eye movements for response. Our results suggest that time and space perception abide by the same algorithm but have different computational properties.

## Introduction

The study of time perception has demonstrated the complex interplay of spatiotemporal information in the brain. As temporal processes are linked to their embodied experience of the environment [1], analyzing the spatial dimension in the study of time perception can provide a powerful tool for understanding the underlying mechanisms that allow us to comprehend the external world. Time and space are two aspects of the physical world that frame our experience of the world. The perception of time and space occurs in an interrelated fashion in human cognition, and recent research shows a growing interest in understanding the underlying mechanisms of their relationship [2–5]. It has been suggested that time perception occurs through spatialization of time intervals in the face of movement-based events of the world [6]. Such spatialization could be seen in the way we have tied the perception of time to space by devising various types of clocks to keep track of the passage of time.

In modern science, time and space have been represented with measurable proxies imbued with operational definitions, i.e., time and distance intervals, respectively [7], which provide a framework for studying and quantifying these abstract concepts. This has made possible the study of the relationship between time and space perception. A variety of time-space interactions in the human perceptual system has been observed. For example, spatiotemporal interference is one such interaction where spatial information can distort the perception of temporal information and vice versa [8]. Peri-saccadic spatiotemporal compression is another phenomenon that serves as evidence of common mechanisms in the perception of time and space [9].

A Theory of Magnitude (ATOM) proposed by Walsh [10] suggests that the brain has a core common magnitude system for time, space, and quantity. According to this theory, the neural mechanisms underlying the perception of time, space, and quantity are intertwined, and the brain

processes these dimensions in a unified manner. This theory has been supported by empirical evidence from studies that have shown that the perception of time and space share common neural substrates [11–16]. A recent meta-analysis of neuroimaging studies [17] has suggested that there is a common system of brain regions that are activated during both time and space processing, including bilateral insula, the pre-supplementary motor area (pre-SMA), the right frontal operculum, and intraparietal sulci. At the neuronal level, it has been observed that spatial information could at least be partially derived from temporal information [18].

Despite these findings, the precise nature and the extent to which these perceptual domains share common mechanisms remain unknown. This has spurred several investigations into better understanding the relationship between time and space [19,20]. Most studies to date have approached the question in terms of the interferences that occur between perceptual domains [21–23]. We attempted to approach this question by utilizing behavioral modeling and model comparison.

A Bayesian understanding of timing has revealed that the interaction of the temporal context and the internal ongoing processes culminates in the calibration of estimated intervals [24] in the form of perceptual biases. Such a formulation of interval timing presents us with two stages in the process of timing, i.e., the measurement (perception) and the reproduction (action) phases of interval timing [25]. The link between the measurement and the reproduction is actualized by an estimation function in the observer model. Based on the nature of the observer model (ideal vs non-ideal), the estimation functions differ. Bayesian least squares (BLS) and maximum likelihood estimation (MLE) estimators have been used in the literature as prior-dependent and prior-independent functions, respectively [25]. The Bayesian perspective has also been explored in human spatial navigation [26,27]. Thus, the probabilistic nature of spatiotemporal information could

be well captured by an optimum-seeking system which combines experience-dependent information with contextual noisy measurements to generate an estimate of various facets of time and space. It remains unclear whether the perceptual biases in time and space are both attributable to the prior information.

In this study, we compared the how spatial and temporal measurements are implemented by probing sources of variability in the process of time and distance measurement and reproduction, within a probabilistic framework. We showed that the perceptual biases in time perception are explained by prior-dependent computations, as previously shown in the literature. On the other hand, we cast doubt on the contribution of prior information to the observed perceptual biases in space perception.

## Results

### Bayesian Observer modeling of time and distance reproduction tasks

We plotted subjects' reproduced time and distance as a function of the presented duration and distance (Fig. 2). In both time and distance, we observed that reproduced time and distance roughly followed the presented time and distance, respectively. In order to observe the goodness-of-fit across our four models ($BLS_{2p}$, $BLS_{3p}$, $MLE_{2p}$, $MLE_{3p}$), we fitted these models to our data, separately, and plotted simulations from the best fitted models on our data. As it is visually evident, the BLS models outperformed MLE models in the time domain. In the distance domain, MLE and BLS models were very similar. We calculated Akaike information criterion (AIC), Bayesian information criterion (BIC), and cross-validated log likelihood (CLL) across subjects for each model. We considered a value of 5 in '2 × difference in CLL' as the cutoff point in model comparison for each pair as was previously suggested. In the time domain, we found that

the $BLS_{3p}$ model is a better fit for 11/20 subjects compared to the other three models (for CLL values, and summary of result, see Table 1). To further investigate the validity of such results, we ran pairwise comparisons of models' CLL values for each subject. These analyses revealed that $BLS_{2p}$ is a better fit than $MLE_{2p}$ in 17/20 subjects (Fig. 3A), $BLS_{3p}$ is a better fit than $MLE_{3p}$ in 19/20 subjects (Fig. 3B), and $BLS_{3p}$ is a better fit than $BLS_{2p}$ in 10/20 subjects (Fig. 3C).

In the distance domain, as it is evident, the 3-paramter models are better fit to the data than the 2-parameter models (Fig. 2B). In 55% of subjects, $BLS_{3p}$ was the best fit among our four models as well (11/20, Table 2). In the pairwise comparisons across models, we observed that in only 2/20 subjects $BLS_{2p}$ was a better fit that $MLE_{2p}$ while in 8/20 subjects, $MLE_{2p}$ was a better fit than $BLS_{2p}$ (Fig. 3D). Comparing $BLS_{3p}$ and $MLE_{3p}$ did not reveal a conclusive picture (Fig. 3E), while $BLS_{3p}$ is a better fit than $BLS_{2p}$ in 11/20 subjects (Fig. 3F). We replicated all of these analyses based on AIC and BIC, and the results were qualitatively similar to CLL data presented here.

**Comparison of model parameters between time and space**

Given our results so far, we compared the best fitted free parameters from $BLS_{3p}$ model between time and space. In the case of α we did not find neither correlation (r = -0.11, p = 0.64, Fig. 4A), nor difference between time (mean ± SD: 1.01 ± 0.21) and space (0.93 ± 0.11; W = 70, $p$ = 0.2, Wilcoxson Rank Sum). We calculated the measurement ($w_m$) and the reproduction ($w_r$) noise parameters of space and time models (Fig. 4B). $w_m$ in space domain (0.05 ± 0.03) was lower than $w_m$ in time domain (0.30 ± 0.07; W = 210, $p < 0.0001$). We also found that $w_r$ in space domain (0.23 ± 0.02) was smaller than $w_r$ in time domain (0.29 ± 0.07; W = 185, $p < 0.001$). We found that although there was no correlation between $w_m$ in space and time domain (r = 0.4, $p$ =

0.08, Fig. 4C), there was a positive and significant correlation between $w_r$ in time and space domain ($r = 0.45$, $p < 0.05$, Fig. 4D).

**Prediction of time/distance intervals across different eccentricities/delays**

In order to see whether time perception was dependent on distance, we fitted $BLS_{3p}$ on the timing data as a function of stimulus eccentricity and used the fitted parameters for simulation across the three eccentricities (6, 8, and 12°). We computed $R^2$ score to assess the goodness-of-fit of a model trained on one eccentricity and tested on other eccentricities. The mean of $R^2$ values is shown in Fig. 5A. As can be seen, although each model from any eccentricities can predict data from other eccentricities well ($R^2$s > 0.83), data from each eccentricity predicted the same eccentricity better than others (the rightward diagonal in Fig. 5A).

In order to see whether distance reproduction was dependent on delay interval, we fitted $BLS_{3p}$ on the space data as a function of delay and used the fitted parameters for simulation across the three delays. We computed $R^2$ score to assess the goodness-of-fit of a model trained on one delay and tested on other delays ($R^2$s > 0.93). The mean of $R^2$ values is shown in Fig. 5B. We did not find any systematic difference between models and data as a function of eccentricity.

## Discussion

We investigated the similarities and differences in the perception of time and space, as two components of the 'A Theory of Magnitude' (ATOM) proposal [10]. Our investigation was motivated by the evidence regarding various encoding schemes that are recruited for time and space across different parts of the brain [19,28,29]. To achieve this goal, we designed two magnitude reproduction tasks and made them as much similar in terms of stimuli and procedure as possible. We used the observer model, which Jazayeri and Shadlen (2010) [25] had used, with two different estimators (Bayesian Least Square (BLS) vs. Maximum Likelihood Estimator (MLE)) to our behavioral data. We showed that adding another parameter ($\alpha$) to the classic Bayesian observer model [25] resulted in better fits regardless of the estimator used. We added $\alpha$ to the ideal Observer model in order to capture the heterogeneity of perception of time and space in population [30].

We showed that in the time domain, models that take priors into account (i.e., $BLS_{2p}$ and $BLS_{3p}$) outperformed those that do not (i.e., $MLE_{2p}$ and $MLE_{3p}$). In the space domain, it remains inconclusive whether $MLE_{3p}$ or $BLS_{3p}$ better captures our data. Since both of these two models in the space domain fitted data well, we chose $BLS_{3p}$ to compare the time and space with the same model. Given that a probabilistic framework explained both time and space, we believe there is a general computation principle in both domains. Our results are corroborated by studies that have shown an effect of global context in time, but not with those that have shown that in space perception [22,24,31]. Although time and space perception abide by shared principles, based on the observed differences between the fitted parameters from time and space models, we believe that this probabilistic computation is applied differently in these two domains: time perception is more prior-dependent, while we cannot say the same for space perception.

Our results are supported by biological evidence as well. A recent meta-analysis has shown that although time and space perception share common regions in the brain, their processing might be separated by an anatomical anterior-posterior gradient [17]. Dissociable neural indices for time and space have also been found in human EEG data [4]. Neural recordings from prefrontal cortex (PFC) and temporal lobe in epileptic patients found neurons that encode time-only, space-only or both time and space. In non-human primates, researchers found that neurons in the PFC that encode time and space have a small overlap with each other [29] and the commonality may be at the level of goal coding. These results can be explained by the recent proposal that the brain uses distinct mechanisms to measure temporal and spatial magnitudes and combines them in a unimodal estimate through another mechanism [32].

In the time domain, we observed in subjects with the lowest and the highest α values, α captured the overall underestimation (Fig. S17) and overestimation (Fig. S3) in time reproduction behavior, respectively. We suggest that α represents the speed of an internal clock [33]. Research has shown that people experience the passage of time in different ways and the speed of the internal clock varies in population [34,35]. In the space domain, we made the same observation regarding α. However, the majority of subjects had α values under 1 (median of 0.9 for the distribution of α) which translates into an overall underestimation tendency in distance reproduction. This observation is in line with previous report of an average undershoot of about 10% of target eccentricity in peripheral saccades [36].

We observed that $w_m$ and $w_r$, model parameters representing the level of variability, were lower in space than in time models. We also found that $w_m$ was not correlated between time and space which hints at the possibility of different measurement mechanisms in the two domains. One explanation for the observed difference in $w_m$ between the two domains could be that there are

various sources of variability for time and space, and the measurement and reproduction of space goes under less noisy stages (or processed further). This difference between time and space can be due to how these dimensions are represented in the brain. We believe that given that brain has many retinotopic maps in which spatial relations such as eccentricity, and distance are coded [37], it has the power to reduce noise at the level of measurement. On the other hand, time has very few chronotopic maps [38], so the perception of time would be subject to more noise than space. At the motor level, it has long been known that the primate brain has a dedicated system for saccadic eye movement that direct eyes to different locations [39]. This system is very precise in transforming static visual scenes into spatiotemporal signals for the brain to structure the spatial maps of the environment [40]. We believe that that is the reason why where to look is less noisy than when to look.

We can compute distance based on information from both egocentric cues (i.e., navigation) and distance from fovea (allocentric, i.e., making a saccade) [41,42,43]. Distance reproduction tasks so far have mostly focused on egocentric representation as studies have been conducted in virtual reality settings [44,45]. We used a task design in which the perceived and reproduced distances represent the allocentric mapping of spatial information. In recent years, research has found that there are neurons that encode egocentric spatial representations and also represent allocentric spatial relations in primate hippocampal formation [46,47] driven by saccadic eye movements during visual exploration of environment [48]. Because of this similarity, we believe our results could generalize to tasks that measure the egocentric encoding of distance.

We observed that as the eccentricity of stimulus increased, the subjects overestimated time intervals, as represented in different (not statistically though) $\alpha$ values obtained from models fitted based on eccentricities we had in our task. We also showed that the fitted parameters to

timing data in different eccentricities are not generalizable to other eccentricities, as shown in the deterioration of the goodness-of-fit metric. This finding is in line with the previous observations that as the distance between two visual stimuli, with a constant stimulus onset asynchrony, increases, the perceived duration between these two stimuli also increases. This effect is known as Kappa [8,49]. On the other hand, the reproduced distances as a function of delay were not different. This observation is unexpected given the literature on the relation of working memory and the anti-saccade task which shows the deterioration of task performance as a function of delay interval [50,51]. We think that the maximum delay duration that we used (1.6 s) is not long enough to manifest the interference effect of time on space.

We do not know that if $BLS_{3p}$ would be a better fit than $BLS_{2p}$ to previously reported data in time domain like the ones from Jazayeri & Shadlen [25]. But although they trained subjects to have a stable performance before their main task, we did not have that training. They also provided feedback regarding the precision of performance to their subjects on each trial, which we did not have that either. So, although we cannot extend our modeling works to theirs, our model is more powerful in dealing with not giving feedback and also not requiring subjects to be heavily trained. Given that our model can accommodate data collection with minimum training, we believe it can be applied more easily to populations that data collection is an obstacle in them, like children or people with neurological or psychiatric disorders.

## Method

### Apparatus

The experiments were carried out on a computer running Linux operating system, on MATLAB (2016b), with Psychtoolbox 3 extension [52]. Stimuli were presented on a monitor (17”) placed ~60 cm from the subject with a 60 Hz refresh rate. The subject sat comfortably on a chair in a dimly lit room to participate in this study, with the head stabilized by a head and chin rest. An EyeLink 1000 infrared eye tracking system (SR Research, Mississauga, Ontario) was used to record eye movements at 1kHz.

### Subjects

We enrolled 22 volunteers (12 female, range: [20, 43], mean ± SD: 26.5 ± 5.5). All were naïve to the purpose of the study except 2 (subjects 1 and 2) who were the authors of this study. We excluded 1 subject because of the troubled eye-tracker calibration caused by her contact lens and 1 subject because of excessively large eye-calibration errors. All subjects had normal or correct-to-normal vision. They had signed the consent form prior to the experiment. The experiment was approved by the ethics committee of the School of Cognitive Sciences (IPM). We counter-balanced all variables and blocks between participants. Half of the participants completed the time reproduction task first. Before starting each experiment, each participant completed a full block of training to familiarize themselves with each task.

### Experiment 1

We designed a time reproduction task in which subjects had to reproduce perceived time intervals. At the beginning of each block, the name of the condition (time) was displayed at the center of the screen. The participant then pressed the space bar to start the block. A white fixation

cross with a length of 0.5° was presented at the center of the screen for 1 second. After participants acquired fixation, a black line was then presented for a variable duration of 500-1000ms (uniform distribution). The participants were instructed to keep their gaze on the fixation point (within a 4° × 4° window). The line extended from the fixation cross to one of the four corners of the screen. The location of the line was fixed within each block, but changed between blocks. After that, a white circle (‘set’, diameter of 1.5°) was flashed on the horizontal meridian, contra-lateral to the black line. The eccentricity of the circle was 6, 8, or 12°, randomly chosen on each trial. After a variable sample interval of 0.4, 0.8, or 1.6 seconds, a white circle (‘go’, diameter of 1.5°) was presented on the black line at the same eccentricity as the flashed circle. Participants were then required to reproduce the duration between the onset of the ‘set’ stimulus and the onset of the ‘go’ stimulus by making a saccade to the ‘go’ target to reproduce the sample interval. If the saccade was landed within a 4° × 4° window of the ‘go’ stimulus, the go stimulus would turn to green (Fig. 1A). We did not provide any feedback regarding the accuracy of the timing. Each block consisted of 54 trials (3 eccentricities, 3 sample interval, and 6 repetitions for each condition) and subjects performed 8 blocks.

**Experiment 2**

We designed the distance reproduction task as similar to the time reproduction task as possible (Fig. 1B). Each trial is similar to the experiment 1 up to the presentation of the ‘set’ stimulus. Here, after passing a variable duration (0.4, 0.8, or 1.6 seconds) from ‘set’ stimulus onset, the fixation cross turned to green (go signal). This indicated to the participants that they should reproduce the distance between the ‘set’ stimulus and the fixation cross by making a saccade to a point on the black line that had the same eccentricity as the ‘set’ stimulus. Gaze locations which landed within 2° of the black line were considered valid. A green circle (diameter of 1.5°) was

presented at the location of the saccade. Each block consisted of 54 trials (3 eccentricities, 3 sample interval, and 6 repetitions for each condition) and subjects performed 8 blocks.

**Data Analysis**

We employed the Interquartile Range (IQR) method as a robust statistical technique to identify and eliminate outlier data points [53]. This method excludes the data that lie outside of 1.5 IQR below the first quantile or 1.5 IQR above the third quantile. We applied the IQR method for each subject for each experiment. We also excluded trials with a reaction time of less than 200 ms The number of excluded trials per subject per experiment was below 1%.

**Ideal Observer model**

In our data, we had pairs of sample time/distance intervals ($t_s$, $d_s$) and corresponding reproduced times/distances ($t_r$, $d_r$) for each trial. We used an ideal observer model to relate sample times/distances to the reproduced ones. To model these relationships, we used two hidden variables, each of which refers to one of the noisy stages of the process of reproducing time/distance intervals. The model has three stages as:

Measurement stage

$$\lambda_{x_m}(x_s) = p(x_m|x_s) = \frac{1}{\sqrt{2\Pi(w_m x_s)^2}} e^{\frac{-(x_s - x_m)^2}{(w_m x_s)^2}}$$

Estimation stage

$$f(x_m) = x_e$$

Reproduction stage

$$p(x_r|x_e) = \frac{1}{\sqrt{2\Pi(w_r x_e)^2}} e^{\frac{-(x_r - x_e)^2}{(w_r x_e)^2}}$$

and then

$$p(x_r|x_s, w_m, w_r) = \int p(x_r|f(x_m), w_r)\, p(x_m|x_s, w_m)\, dx_m$$

x stands for t (parameters from the time reproduction task) or d (parameters from the space reproduction task)

For the time reproduction task, we have $t_s$, sample time interval; $t_m$, measured time interval; $t_r$, reproduced time interval; $t_e$, estimated time interval; $w_m$, measurement Weber fraction; $w_r$, reproduction weber fraction. For the distance reproduction task, we have $d_s$ sample distance interval, $d_m$, measured distance interval, $d_r$, reproduced distance interval, and, $d_e$, estimated distance interval.

In these observer models, $p(t_m|t_s)$ and $p(d_m|d_s)$ are modeled as Gaussian distributions centered at $t_s$ and $d_s$, and we assume that their standard deviations (SD) grow linearly with their means. This assumption is motivated by the scalar variability of timing and distance [25,27]. The distribution of measurement noise is thus fully characterized by the ratio of the SD to the mean of $p(t_m|t_s)$ and $p(d_m|d_s)$, which we will refer to as the Weber fraction associated with the measurement, $w_m$. With the same arguments in mind, we assume that the distributions of $t_r$ and $d_r$ conditioned on $t_e$ and $d_e$, $p(t_r|t_e)$ and $p(d_r|d_e)$, are also Gaussian, centered at $t_e$ and $d_e$, and associated with a constant Weber fraction, $w_r$. We used a Maximum Likelihood Estimation (MLE) function, which does not fuse prior information with the likelihood function, and a

Bayesian Least Squares (BLS) function in the estimation stage of both tasks. For the Bayesian models, we used a uniform distribution over the range of experimental $x_s^{min}$ and $x_s^{max}$. The BLS and MLE functions were defined as:

$$f_{BLS}(x_m) = \frac{\int_{x_s^{min}}^{x_s^{max}} x_s p(x_m|x_s)\, dx_s}{\int_{x_s^{min}}^{x_s^{max}} p(x_m|x_s)\, dx_s}$$

$$f_{MLE}(x_m) = \underset{x_s}{argmax}\ \lambda_{x_m}(x_s) = x_m \left[\frac{-1+\sqrt{1+4{w_m}^2}}{2{w_m}^2}\right]$$

In the pilot data, we observed individual-specific shifts in the range effect as represented in an overall tendency to over/under-estimate across the whole range of intervals. These patterns were not explained by the common observer model so we used a modified version of these models. We introduced another free parameter (α) to the estimation stage of the model as a multiplication factor. So, the estimation stage for these models would be:

$$f_{BLS}(x_m) = \frac{\int_{x_s^{min}}^{x_s^{max}} \boldsymbol{\alpha}\,.\, x_s p(x_m|x_s)\, dx_s}{\int_{x_s^{min}}^{x_s^{max}} p(x_m|x_s)\, dx_s}$$

$$f_{MLE}(x_m) = \underset{x_s}{argmax}\ \lambda_{x_m}(x_s) = \boldsymbol{\alpha}\,.\, x_m \left[\frac{-1+\sqrt{1+4{w_m}^2}}{2{w_m}^2}\right]$$

In a separate analysis, we added α to the estimation stage as an additive parameter. The result from multiplication and addition did not differ from each other qualitatively, so we only showed

the multiplicative modulation. We preferred the multiplication result as it gives us a unitless α which is comparable between our tasks.

**Model fitting**

We maximized the likelihood of model parameters $w_m$, $w_r$, and α (when applicable) across all $x_s$ and $x_r$ values. Maximum likelihood estimation was performed with the minimize function in SciPy library, using the Nelder-Mead downhill simplex optimization method. We evaluated the success of the fitting procedure by repeating the search with several different initial values.

**Model comparison**

In order to compare modified models (with α) with the previous models (without α), we used Akaike Information Criterion (AIC), Bayesian Information Criterion (BIC), and Cross-validated Log-Likelihoods (CLL) as our quantitative criteria. We also plotted the averaged result of 50 simulations of tasks with the best fitted models over the data. We compared plots to make sure there are visible differences between the models. We also wanted to check that the best model actually captures the pattern of the data well. We considered differences bigger than 5 in each criterion (i.e., AIC, BIC, and CLL) between different models, as an indicator of better model performance [54]. We also used the highest CLL values among the models as an absolute measure of goodness-of-fit. We performed comparisons between the modified and the classic models, separately for $f_{BLS}$ and $f_{MLE}$ estimators, to choose the best model for time and space reproduction, again separately.

**Difference between model parameters of time and space**

We employed Wilcoxon signed-rank test to detect possible differences between model parameters ($\alpha$, $w_m$, and $w_r$) obtained from the best fitted $BLS_{3p}$ model between time and space. We considered p-values of less than 0.05 as an indication of statistical significance.

**Correlation between time and space**

We calculated Pearson correlation between the best fitted model parameters for the time and distance reproduction tasks to measure the degree of potential overlap between time and distance perception.

**Prediction of a perceptual domain as a function of another one**

We fitted $BLS_{3p}$ on the time and distance data as a function stimulus eccentricity and fixation to GO delay, respectively. We computed $R^2$ score to assess the goodness-of-fit of a model trained on one eccentricity/delay and tested on other eccentricities/delays. Since we wanted to see how the overall performance of our model in capturing the mean and SD of data across different eccentricities/delays changes, we used the mean predicted values and the true values across time and distance intervals to calculate $R^2$ for each subject. With this approach we had the problem of small number of sample points (3 in each domain) which resulted in negative $R^2$ values in some of the train-test combinations in time domain for 5 subjects. We excluded these 5 subjects from this analysis in time domain.

**Data Availability**

Data and code will be published upon acceptance of the paper.

**Acknowledgments**

We are grateful to Abdol-hossein Vahabie for giving feedback on our data analysis approach, and Mohammad Rabie for comments on a previous version of our manuscript.

**Competing interests**

The authors declare no competing interests

## References


1. Safaie, M. *et al.* Turning the body into a clock: Accurate timing is facilitated by simple stereotyped interactions with the environment. *Proceedings of the National Academy of Sciences* **117**, 13084–13093 (2020).
2. Whitaker, M. M., Hansen, R. C., Creem-Regehr, S. H. & Stefanucci, J. K. The relationship between space and time perception: A registered replication of Casasanto and Boroditsky (2008). *Atten Percept Psychophys* **84**, 347–351 (2022).
3. Schroeger, A., Raab, M. & Cañal-Bruland, R. Tau and kappa in interception – how perceptual spatiotemporal interrelations affect movements. *Atten Percept Psychophys* **84**, 1925–1943 (2022).
4. Robinson, E. M. & Wiener, M. Dissociable neural indices for time and space estimates during virtual distance reproduction. *NeuroImage* **226**, 117607 (2021).
5. Goldreich, D. A Bayesian Perceptual Model Replicates the Cutaneous Rabbit and Other Tactile Spatiotemporal Illusions. *PLOS ONE* **2**, e333 (2007).
6. Robbe, D. Lost in time: Relocating the perception of duration outside the brain. *Neuroscience & Biobehavioral Reviews* **153**, 105312 (2023).
7. Buzsáki, G. & Llinás, R. Space and time in the brain. *Science* **358**, 482–485 (2017).
8. Vidaud-Laperrière, K., Brunel, L., Syssau-Vaccarella, A. & Charras, P. Exploring spatiotemporal interactions: On the superiority of time over space. *Atten Percept Psychophys* **84**, 2582–2595 (2022).
9. Morrone, M. C., Ross, J. & Burr, D. Saccadic eye movements cause compression of time as well as space. *Nat Neurosci* **8**, 950–954 (2005).
10. Walsh, V. A theory of magnitude: common cortical metrics of time, space and quantity. *Trends in Cognitive Sciences* **7**, 483–488 (2003).
11. Cai, Z. G. & Connell, L. On magnitudes in memory: An internal clock account of space–time interaction. *Acta Psychologica* **168**, 1–11 (2016).

380 12. Casasanto, D. & Boroditsky, L. Time in the mind: Using space to think about time. *Cognition* **106**,
381 579–593 (2008).
382 13. Chen, Y., Peng, C. & Avitt, A. A unifying Bayesian framework accounting for spatiotemporal
383 interferences with a deceleration tendency. *Vision Research* **187**, 66–74 (2021).
384 14. Cui, M., Peng, C., Huang, M. & Chen, Y. Electrophysiological evidence for a common magnitude
385 representation of spatiotemporal information in working memory. *Cerebral Cortex* **32**, 4068–4079
386 (2022).
387 15. Howard, M. W. *et al.* A Unified Mathematical Framework for Coding Time, Space, and Sequences in
388 the Hippocampal Region. *J. Neurosci.* **34**, 4692–4707 (2014).
389 16. Jie, Y. U. & Youguo, C. Spatiotemporal interference effect: An explanation based on Bayesian models.
390 *Advances in Psychological Science* **31**, 597 (2023).
391 17. Cona, G., Wiener, M. & Scarpazza, C. From ATOM to GradiATOM: Cortical gradients support time and
392 space processing as revealed by a meta-analysis of neuroimaging studies. *NeuroImage* **224**, 117407
393 (2021).
394 18. Burgess, C., Schuck, N. W. & Burgess, N. Chapter 5 - Temporal Neuronal Oscillations can Produce
395 Spatial Phase Codes. in *Space, Time and Number in the Brain* (eds. Dehaene, S. & Brannon, E. M.)
396 59–69 (Academic Press, San Diego, 2011). doi:10.1016/B978-0-12-385948-8.00005-0.
397 19. Abramson, S. *et al.* Flexible coding of time or distance in hippocampal cells. *eLife* **12**, e83930 (2023).
398 20. Schonhaut, D. R., Aghajan, Z. M., Kahana, M. J. & Fried, I. A neural code for time and space in the
399 human brain. *Cell Reports* **42**, 113238 (2023).
400 21. Marcos, E. & Genovesio, A. Interference between Space and Time Estimations: From Behavior to
401 Neurons. *Frontiers in Neuroscience* **11**, (2017).
402 22. Martin, B., Wiener, M. & van Wassenhove, V. A Bayesian Perspective on Accumulation in the
403 Magnitude System. *Sci Rep* **7**, 630 (2017).

23. Üstün, S., Sırmatel, B. & Çiçek, M. Can a Common Magnitude System Theory Explain the Brain Representation of Space, Time, and Number? *Noro Psikiyatr Ars* **59**, S24–S28 (2022).
24. Sadibolova, R. & Terhune, D. B. The temporal context in bayesian models of interval timing: Recent advances and future directions. *Behav Neurosci* **136**, 364–373 (2022).
25. Jazayeri, M. & Shadlen, M. N. Temporal context calibrates interval timing. *Nat Neurosci* **13**, 1020–1026 (2010).
26. Petzschner, F. H. & Glasauer, S. Iterative Bayesian Estimation as an Explanation for Range and Regression Effects: A Study on Human Path Integration. *J. Neurosci.* **31**, 17220–17229 (2011).
27. Thurley, K. & Schild, U. Time and distance estimation in children using an egocentric navigation task. *Sci Rep* **8**, 18001 (2018).
28. Kraus, B. J., Robinson, R. J., White, J. A., Eichenbaum, H. & Hasselmo, M. E. Hippocampal 'time cells': time versus path integration. *Neuron* **78**, 1090–1101 (2013).
29. Marcos, E., Tsujimoto, S. & Genovesio, A. Independent coding of absolute duration and distance magnitudes in the prefrontal cortex. *Journal of Neurophysiology* **117**, 195–203 (2017).
30. Matthews, W. J. & Meck, W. H. Time perception: the bad news and the good. *Wiley Interdiscip Rev Cogn Sci* **5**, 429–446 (2014).
31. Wang, T. *et al.* A unitary mechanism underlies adaptation to both local and global environmental statistics in time perception. *PLOS Computational Biology* **19**, e1011116 (2023).
32. Gladhill, K. A., Robinson, E. M., Stanfield-Wiswall, C., Bader, F. & Wiener, M. Anchors for Time, Distance, and Magnitude in Virtual Movements. 2022.09.12.507649 Preprint at https://doi.org/10.1101/2022.09.12.507649 (2022).
33. Meck, W. H. Selective adjustment of the speed of internal clock and memory processes. *J Exp Psychol Anim Behav Process* **9**, 171–201 (1983).

34. Allman, M. J., Teki, S., Griffiths, T. D. & Meck, W. H. Properties of the Internal Clock: First- and Second-Order Principles of Subjective Time. *Annual Review of Psychology* **65**, 743–771 (2014).

35. Wearden, J. H., Philpott, K. & Win, T. Speeding up and (…relatively…) slowing down an internal clock in humans. *Behavioural Processes* **46**, 63–73 (1999).

36. Vitu, F., Casteau, S., Adeli, H., Zelinsky, G. J. & Castet, E. The magnification factor accounts for the greater hypometria and imprecision of larger saccades: Evidence from a parametric human-behavioral study. *Journal of Vision* **17**, 2 (2017).

37. Felleman, D. J. & Van Essen, D. C. Distributed hierarchical processing in the primate cerebral cortex. *Cereb Cortex* **1**, 1–47 (1991).

38. Protopapa, F. *et al.* Chronotopic maps in human supplementary motor area. *PLoS Biol* **17**, e3000026 (2019).

39. Rucci, M., Iovin, R., Poletti, M. & Santini, F. Miniature eye movements enhance fine spatial detail. *Nature* **447**, 851–854 (2007).

40. Rucci, M. & Poletti, M. Control and Functions of Fixational Eye Movements. *Annual Review of Vision Science* **1**, 499–518 (2015).

41. Feigenbaum, J. D. & Rolls, E. T. Allocentric and egocentric spatial information processing in the hippocampal formation of the behaving primate. *Psychobiology* **19**, 21–40 (1991).

42. Sabes, P. N., Breznen, B. & Andersen, R. A. Parietal Representation of Object-Based Saccades. *Journal of Neurophysiology* **88**, 1815–1829 (2002).

43. Olson, C. R. Brain representation of object-centered space in monkeys and humans. *Annu Rev Neurosci* **26**, 331–354 (2003).

44. Zhang, J., Yang, X., Jin, Z. & Li, L. Distance Estimation in Virtual Reality Is Affected by Both the Virtual and the Real-World Environments. *i-Perception* **12**, 20416695211023956 (2021).

45. Maruhn, P., Schneider, S. & Bengler, K. Measuring egocentric distance perception in virtual reality: Influence of methodologies, locomotion and translation gains. *PLoS One* **14**, e0224651 (2019).
46. Courellis, H. S. *et al.* Spatial encoding in primate hippocampus during free navigation. *PLOS Biology* **17**, e3000546 (2019).
47. Baraduc, P., Duhamel, J.-R. & Wirth, S. Schema cells in the macaque hippocampus. *Science* **363**, 635–639 (2019).
48. Killian, N. J., Jutras, M. J. & Buffalo, E. A. A map of visual space in the primate entorhinal cortex. *Nature* **491**, 761–764 (2012).
49. Jones, B. & Huang, Y. L. Space-time dependencies in psychophysical judgment of extent and duration: Algebraic models of the tau and kappa effects. *Psychological Bulletin* **91**, 128–142 (1982).
50. Munoz, D. P. & Everling, S. Look away: the anti-saccade task and the voluntary control of eye movement. *Nat Rev Neurosci* **5**, 218–228 (2004).
51. Meier, M. E., Smeekens, B. A., Silvia, P. J., Kwapil, T. R. & Kane, M. J. Working Memory Capacity and the Antisaccade Task: A Microanaltyic-Macroanalytic Investigation of Individual Differences in Goal Activation and Maintenance. *J Exp Psychol Learn Mem Cogn* **44**, 68–84 (2018).
52. Brainard, D. H. The Psychophysics Toolbox. *Spat Vis* **10**, 433–436 (1997).
53. Schwertman, N. C., Owens, M. A. & Adnan, R. A simple more general boxplot method for identifying outliers. *Computational Statistics & Data Analysis* **47**, 165–174 (2004).
54. Ma, W. J., Kording, K. P. & Goldreich, D. *Bayesian Models of Perception and Action: An Introduction*. (MIT press, 2023).

## Tables

**Table 1.** Cross-validated log-likelihoods (CLL) computed for models with BLS3p, MLE3p, BLS2p, and MLE2p estimators in *time* domain for all subjects. Bold values represent the highest value among the 4 models.

| Subject ID | $BLS_{3p}$ CLL | $MLE_{3p}$ CLL | $BLS_{2p}$ CLL | $MLE_{2p}$ CLL |
|---|---|---|---|---|
| 1 | **-3.15** | -18.11 | -3.18 | -13.04 |
| 2 | **-2.25** | -12.43 | -3.29 | -13.98 |
| 3 | **-10.25** | -22.42 | -27.13 | -29.24 |
| 4 | **-12.78** | -24.46 | -12.80 | -28.80 |
| 5 | **-9.62** | -11.66 | -10.92 | -15.25 |
| 6 | **-3.98** | -16.92 | -4.65 | -20.13 |
| 7 | **-9.22** | -14.75 | -10.41 | -20.36 |
| 8 | **-6.99** | -16.43 | -12.85 | -20.84 |
| 9 | **-23.69** | -30.02 | -28.00 | -35.54 |
| 11 | **13.18** | -0.13 | 3.67 | -0.12 |
| 12 | **-21.10** | -30.93 | -21.68 | -38.66 |
| 13 | **-0.74** | -15.14 | -0.99 | -18.87 |
| 14 | **-22.69** | -37.52 | -25.97 | -46.03 |
| 15 | **14.81** | 3.78 | -4.38 | 0.70 |
| 16 | **-11.70** | -23.43 | -15.21 | -24.95 |
| 17 | **-3.50** | -18.55 | -6.61 | -20.16 |
| 18 | **-0.01** | -4.06 | -12.73 | -5.64 |
| 19 | **8.84** | -5.20 | 8.54 | -11.45 |
| 21 | **-16.23** | -24.39 | -16.18 | -28.24 |
| 22 | **-15.24** | -23.37 | -26.14 | -36.31 |

**Table 2.** Cross-validated log-likelihoods (CLL) computed for models with BLS3p, MLE3p, BLS2p, and MLE2p estimators in *space* domain for all subjects. Bold values represent the highest value among the 4 models.

| Subject ID | $BLS_{3p}$ CLL | $MLE_{3p}$ CLL | $BLS_{2p}$ CLL | $MLE_{2p}$ CLL |
|---|---|---|---|---|
| 1 | **-78.00** | -78.68 | -86.05 | -81.82 |
| 2 | -88.40 | **-87.93** | -89.34 | -88.96 |
| 3 | -83.91 | -83.95 | -89.30 | -89.21 |
| 4 | **-65.21** | -66.82 | -68.74 | -67.30 |
| 5 | **-71.45** | -71.98 | -79.79 | -75.68 |
| 6 | **-87.20** | -87.36 | -89.35 | -89.77 |
| 7 | **-74.52** | -74.70 | -86.35 | -80.89 |
| 8 | -73.72 | **-73.43** | -84.51 | -79.44 |
| 9 | **-84.95** | -85.72 | -86.78 | -85.73 |
| 11 | **-76.33** | -77.00 | -89.62 | -83.65 |
| 12 | -78.45 | **-77.45** | -82.12 | -78.78 |
| 13 | **-68.91** | -69.53 | -70.23 | -69.40 |
| 14 | **-82.18** | -85.35 | -82.21 | -85.96 |
| 15 | -66.76 | **-66.51** | -67.17 | -67.13 |
| 16 | -73.24 | **-73.11** | -82.57 | -77.87 |
| 17 | **-80.69** | -81.06 | -81.30 | -81.90 |
| 18 | -90.48 | -89.11 | -90.48 | **-88.98** |
| 19 | **-81.45** | -83.86 | -83.51 | -87.70 |
| 21 | -78.63 | **-77.78** | -81.33 | -78.79 |
| 22 | -74.77 | **-74.36** | -93.85 | -84.76 |

## Figure Legends

**Figure 1.** The sequence of trial events for the time reproduction task **(A)** and the distance reproduction task **(B)**. **(A),** Participants were given a time reproduction task in which they had to reproduce sample time intervals. After acquiring fixation and the presentation of a black line on screen, A white circle ('set') appeared on the horizontal meridian of the screen, and after a sample interval, another white circle ('go') appeared on the black line. Participants had to reproduce the sample interval by making a saccade to the 'go' stimulus. Successful saccades turned the 'go' stimulus green, but no timing feedback was provided. **(B),** A distance reproduction task was designed similarly to the time reproduction task. It involved the same setup until the appearance of the 'set' stimulus. In this case, participants had to reproduce the distance between the 'set' stimulus and the fixation cross by making a saccade to a point on the black line at the same eccentricity as the 'set' stimulus. Valid saccades were marked with a green circle, and each block consisted of 54 trials with variations in eccentricity and sample intervals.

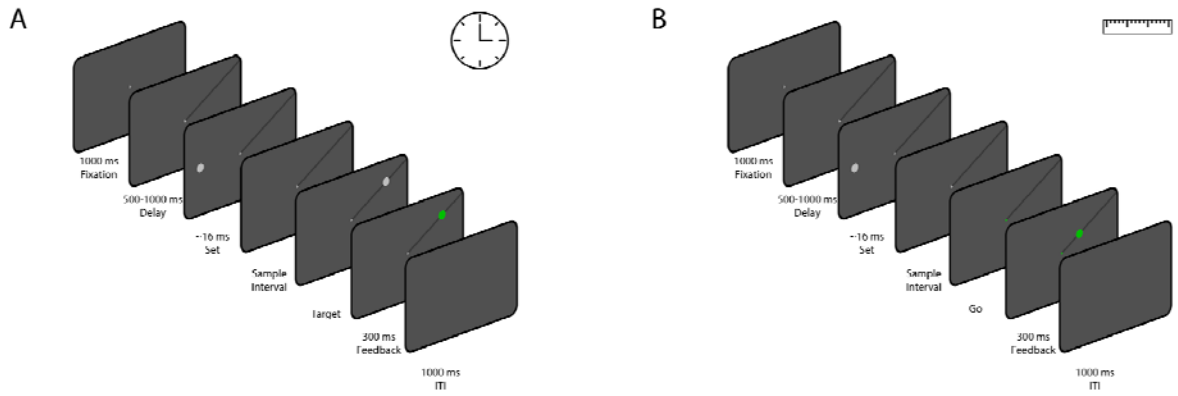


**Figure 2.** Subjects and observer model behavior in time reproduction **(A)** and distance reproduction tasks **(B)**. **(a1-a4),** Black circles and the error bar show the mean ± SD of subjects' reproduced times across three sample intervals. The colored circles and the dotted error bar indicate the mean ± SD of the Bayesian Observer model reproduced times computed from simulations of the best-fitted models with 4 estimators ($BLS_{3p}$, $BLS_{2p}$, $MLE_{3p}$, $MLE_{2p}$, respectively). **(b1-b4),** Black circles and the error bar show the mean ± SD of subjects' reproduced distances across three sample intervals. The colored circles and the dotted error bar indicate the mean ± SD of the Bayesian Observer model reproduced distances computed from simulations of the best-fitted models with 4 estimators, $BLS_{2p}$, $BLS_{3p}$, $MLE_{2p}$, and $MLE_{3p}$, respectively. The inset in **(a2, a4, b2, b4)** shows the distribution of alpha values for all subjects. The dotted line represents the median of alpha distribution.

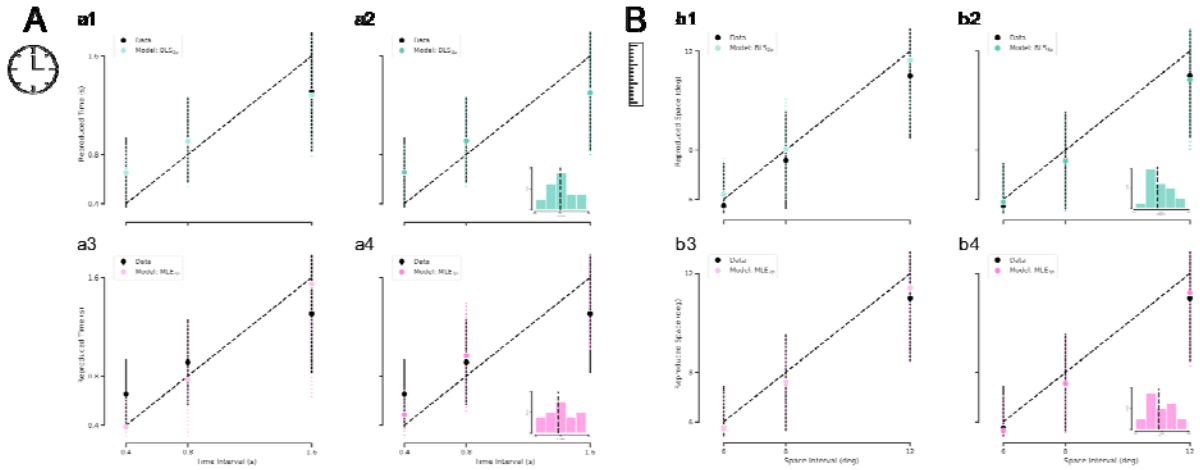


**Figure 3.** Pair-wise comparisons of observer models with different estimators in time and space. **(A, B)** Cross-validated log-likelihoods (CLL) were multiplied by 2 and the relative differences of $BLS_{2p}$ (light green) and $BLS_{3p}$ (dark green) models to $MLE_{2p}$ (light pink) and $MLE_{3p}$ (dark pink) models in time domain are plotted respectively in **(A)** and **(B)**. **(C)** CLLs were multiplied by 2 and the relative differences of $BLS_{3p}$ (dark green) model to $BLS_{2p}$ (light green) model in time domain is plotted. **(D, E)** CLLs were multiplied by 2 and the relative differences of $BLS_{2p}$ (light green) and $BLS_{3p}$ (dark green) models to $MLE_{2p}$ (light pink) and $MLE_{3p}$ (dark pink) models in space domain are plotted respectively in **(D)** and **€**. **(F)** CLLs were multiplied by 2 and the relative differences of $BLS_{3p}$ (dark green) model to $BLS_{2p}$ (light green) model in space domain is plotted. Ordinate represents subject's ID in each subplot.

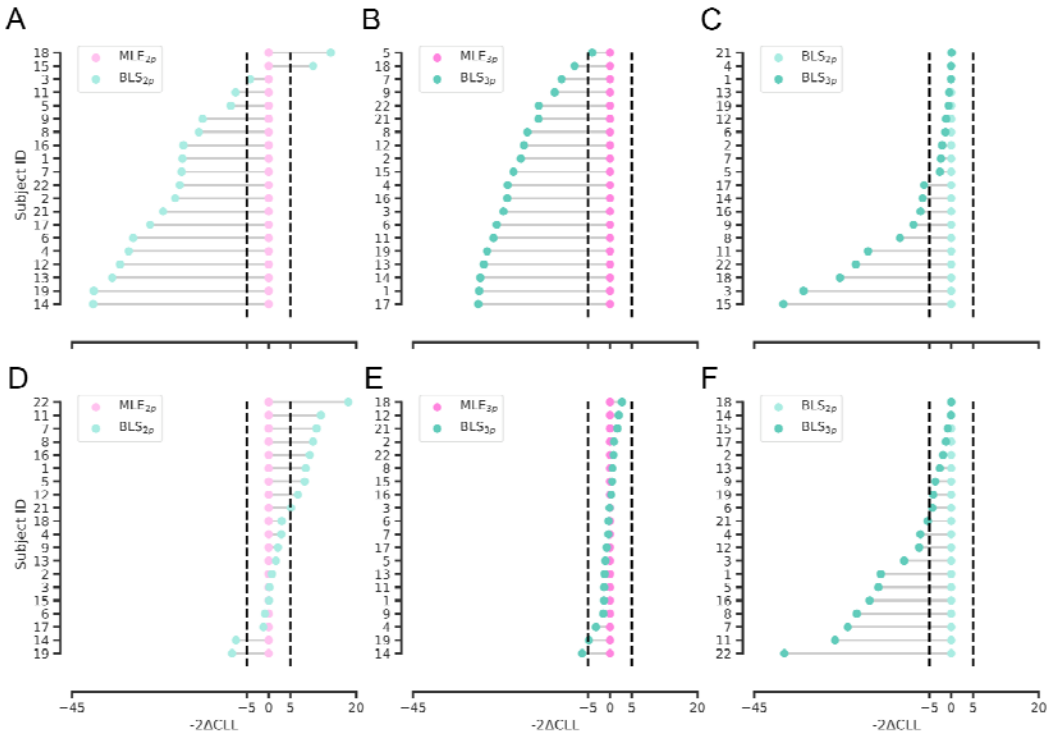


**Figure 4.** Comparison of and correlation between best fitted model parameters computed in time and space. **(A)** The correlation (r = -0.11, p = 0.64) between alpha computed from the $BLS_{3p}$ model in time and space. **(B)** Box plot comparing the distribution of best-fitted model noise parameters between time and space. The line inside the box represents the median, and the whiskers extend to the most extreme data points within 1.5 times the inter-quartile range (IQR). The Wilcoxon signed rank test was conducted to assess the statistical significance of the differences between best-fitted model noise parameters in time and space. $p < 0.001$***, $p < 0.0001$****. **(C)** The correlation (r = 0.40, p = 0.08) between computed from the $BLS_{3p}$ model in time and space. **(D)** The correlation (r = 0.45, p < 0.05) between computed from the $BLS_{3p}$ model in time and space.

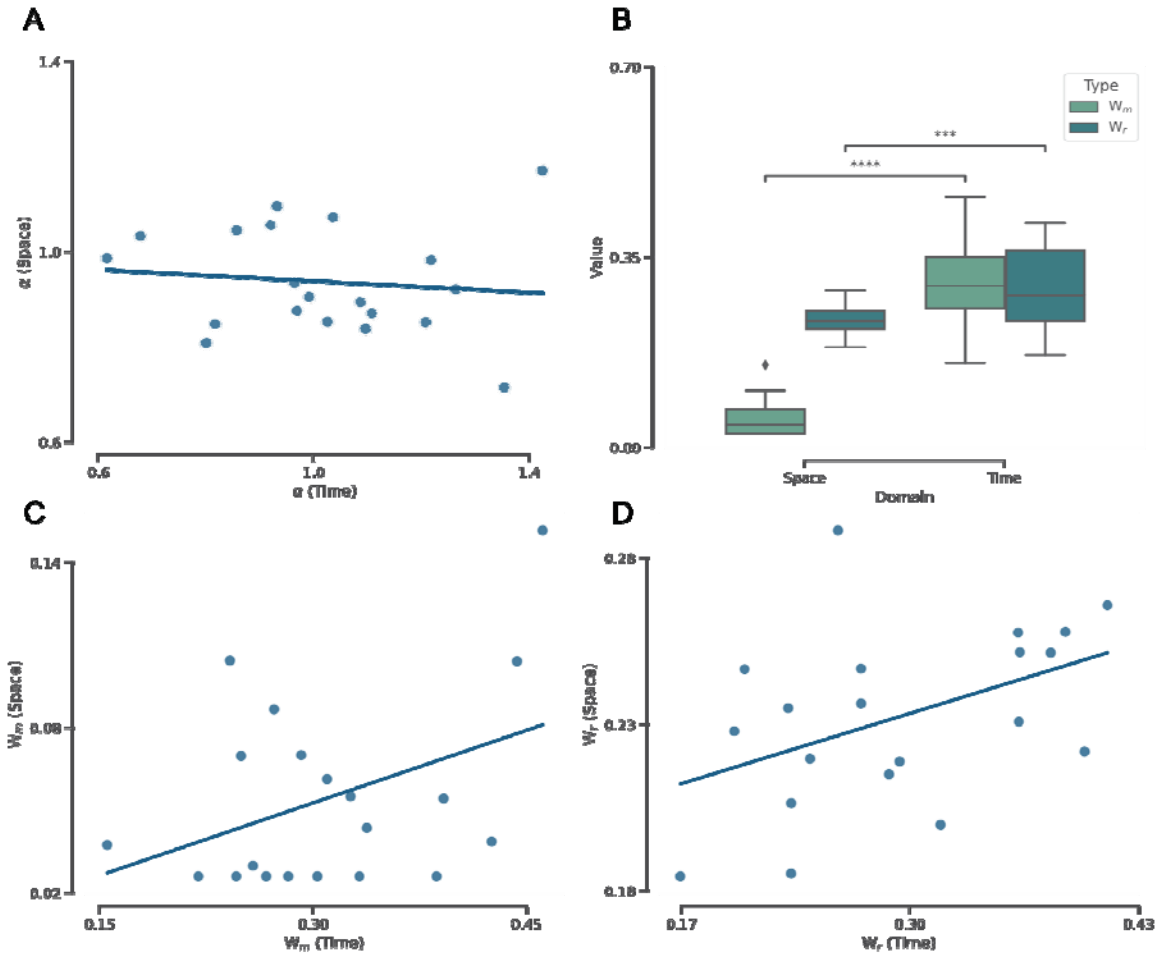


**Figure 5.** Prediction of a perceptual domain as a function of another one. **(A)** Heatmap shows $R^2$ values for the simulated Bayesian Observer model ($BLS_{3p}$) for time domain fitted on trials with short (6°), inter (8°), and long (12°) stimulus eccentricity and tested on trials with these eccentricities. **(B)** Heatmap shows $R^2$ values for the simulated Bayesian Observer model ($BLS_{3p}$) for distance fitted on trials with short (0.4 s), inter (0.8 s), and long (1.6 s) fixation to GO delays and tested on trials with these delays.

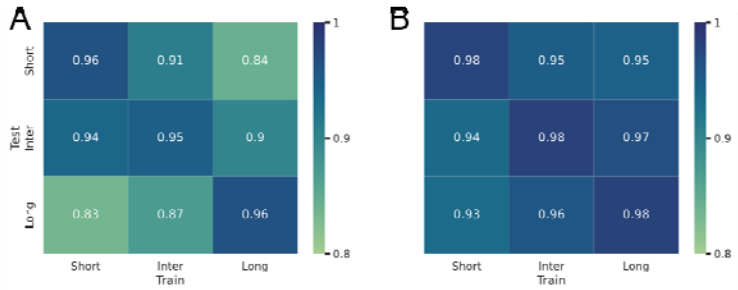

**Figure S1-S20.** Subject and observer model behavior in time reproduction (Up) and in distance reproduction (Down).